ACS OMEGA

http://pubs.acs.org/journal/acsodf

Article

Phosphorus-Containing Flame-Retardant Benzocyclobutylene Composites with High Thermal Stability and Low CTE

Chao Guo, Qiuxia Peng, Hubo Wei, Jiaying Liu, Xinyu Hu, Juan Peng, Jiajun Ma,* Xu Ye,* and Junxiao Yang

Cite This: *ACS Omega* 2023, 8, 9464−9474

Read Online

ACCESS | Metrics & More | Article Recommendations | Supporting Information

ABSTRACT: As a component of printed circuit substrate, copper clad laminate (CCL) needs to meet the performance requirements of heat resistance, flame retardancy, and low coefficient of thermal expansion (CTE), which, respectively, affects the stability, safety, and processability of terminal electronic products. In this paper, benzocyclobutylene (BCB)-functionalized phosphorus−oxygen flame retardant composites were prepared through introducing the BCB groups, and the performance was researched by thermogravimetric analysis, microcombustion calorimetry, and thermomechanical analysis. The research results show that these phosphorus oxide compounds containing BCB groups show good thermal stability and low total heat release (THR) after thermal curing, and the more BCB groups on the phosphorus oxide monomers, the better the thermal stability and flame retardancy of cured resins. The T_{d5} and THR of the composite (M3) are as high as 443 °C and 23.1 kJ/g, respectively. In addition, the CTE of M3 is as low as 16.71 ppm/°C. Introduction of BCB groups which can be crosslinked through heat to improve the thermal stability, flame retardancy, and reduced CTE of traditional organophosphorus flame retardant materials. These materials are expected to be good candidates for CCL substrates for electronic circuits.

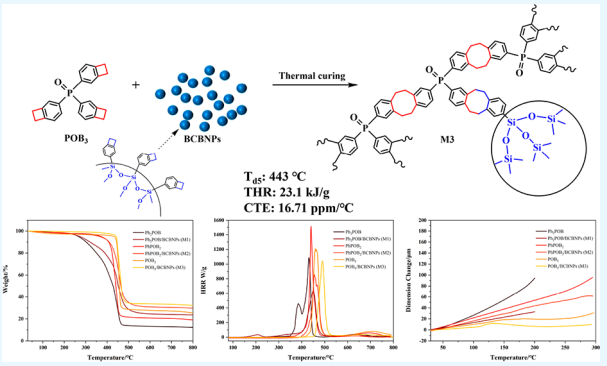

1. INTRODUCTION

CCL is a product made by dipping paper, glass cloth, and other reinforcing materials in resin (such as epoxy resin, polyester resin, and cyanate resin), coating the copper foil on one or both sides, and hot pressing. As a substrate material in the manufacturing of printed circuit boards, CCL plays an important role in interconnecting, conducting, insulating, and supporting the printed circuit boards.[1,2] In recent years, modern communication equipment has developed toward the direction of high integration density and high-frequency 5G. It requires not only CCL with low dielectric constant (D_k) and low dielectric loss (D_f) but also certain thermal stability, flame retardancy, and low CTE to meet the requirements of preparation and use. However, the traditional CCL based on epoxy resin can no longer meet these requirements.[3−5] Initially, CCL achieved the goal of flame retardancy by adding halogen-containing ingredients (mainly bromine and chlorine) to the system. But such materials will cause pollution and post-treatment difficulties, so they are not environmentally friendly materials and are being phased out gradually.[6] It is the reason that researchers turn their attention to the field of phosphorus-containing flame retardant materials. Among them, the specific chemical structure of organophosphorus flame retardants (OPFRs) determines their advantages. For example, Ai et al[7] reported that layered phosphorus-bridged amide-additive flame retardants have the characteristics of low smoke and low toxicity. Bruchajzer et al[8] reported that OPFRs are not stable compounds. They are metabolized and rapidly excreted from the body, proving their low toxicity. Wendels et al[9] reviewed the development of OPFRs in recent years. They believed that some common synthesis methods, such as the Michael addition, Friedel−Crafts reaction, and Michaelis−Arbuzov reaction, can be industrially exploited in industry, considering that their advantages, like higher yields, selectivity, and simplicity of reaction could be used to synthesize new P−C structures, which will have a lot of potential applications as flame retardants and various polymers in the future. At the same time, Du et al[10] reported the impact of OPFRs in environmental risk assessment. They believed that it is very important to systematically understand the toxicity of OPFRs to prevent its use. Meanwhile, it is necessary to solve the current knowledge gap about OPFRs to determine human health hazards and assess environmental risks. The develop-

Received: December 23, 2022
Accepted: February 17, 2023
Published: March 1, 2023

ment and application of new OPFR structures should conform to the environmental development direction of low pollution from flame-retardant materials. Therefore, OPFRs have great development potential and space. In order to meet the needs of certain specific applications,[11−13] they have received continuous attention from flame retardant researchers at home and abroad. For example, the representative of OPFRs are 9,10-dihydro-9-oxa-10-phosphazephenanthrene-10-oxide and its derivatives, which are characterized by the rigid structure of the benzene ring, high rigidity, high heat resistance, good flame retardancy, and low toxicity, which are widely used in the CCL field to improve their flame retardance.[14]

As one of the most common traditional CCLs, the epoxy resin glass laminate has attracted extensive attention due to its relatively acceptable dielectric properties, good stability, and processability.[15] In recent years, with the rapid development of miniaturization and wearability of modern communication equipment, new requirements have been put forward for the machinability of CCL, which requires not only certain mechanical properties as support but also low CTE to ensure that CCL will not deform or break during processing, resulting in performance damage.[16] At the same time, the CTE between materials and copper foils in CCL is also worth paying attention to. Excessive differences in CTE between the two will lead to interlayer delamination of copper foils during operation at high frequency or power and high temperature, which will deform from the CCL substrate during application.[17−19] This will reduce the reliability and service life of CCL and in some cases lead to catastrophic equipment failure. The high CTE of the substrate usually weakens the stability of the CCL through-hole. Severe shrinkage or expansion usually causes the through-hole to break, thus damaging the circuit during heat treatment. This requires the materials in CCL to be close to the CTE of copper foil, so as to have good dimensional stability. The CTE to reduce CCL can be added with low-CTE organic monomers (such as alkoxysilyl-functionalized resin) or negative-CTE organic monomers (such as dibenzocyclooctane) or use low-CTE resin materials (such as cyanate ester resin).[20−23]

The introduction of highly crosslinked polymers in CCL can not only improve its thermal stability and dimensional stability but also effectively reduce its dielectric constant. For example, 1,2-polybutadiene (1,2 PB),[24] styrene butadiene styrene triblock copolymer (SBS),[25] and ethylene propylene dicyclopentadiene[26] are ideal polymer matrices for CCL because they have good thermal stability through the formation of cross-linked structures. Benzocyclobutylene (BCB) is an all-hydrocarbon low-dielectric material with a simple and symmetrical structure, low polarity, and a low possibility of polarization to form a dipole, which makes the cured BCB resin have good thermal stability and a low dielectric constant so it can be used in microelectronics, large-scale integrated circuits, and other fields.[27] Without any catalyst or additive, BCB's unique four-membered ring structure undergoes a ring-opening isomerization reaction after being heated. The highly active intermediate orthoquinone can immediately self-cross-connect with itself to form a benzo eight-membered ring structure.[28] It can also react with materials containing unsaturated bonds to form a benzo six-membered ring structure. Small molecules will not be produced during the curing process, which will not affect the process and the internal structure of the resin. At the same time, due to the highly cross-linked structure after curing,[29−31] the cured resin usually has good thermal stability[32] and good dimensional stability.[33] Meanwhile, the benzene ring contained in the BCB monomer is a rigid structure, which can provide certain mechanical properties to the resin and has a certain elastic modulus and hardness. It has been widely studied and applied as an electronic packaging material and a high-density CCL substrate.

In this paper, our aim is to prepare a kind of thermosetting resin with its own flame retardancy to solve the problem that traditional epoxy resins need to add additional flame retardants to achieve flame retardancy. Therefore, we combine the advantages of OPFR materials and BCB to synthesize phosphorus oxide monomers with different amounts of BCB groups in order to research the effects of the introduction of BCB groups on the thermal stability, flame retardancy, CTE, and mechanical properties of organophosphorus materials by controlling the crosslinking density of the resin. In addition, three monomers were doped with BCB-functionalized spherical silicon nanoparticles (BCBNPs) of the same proportion to prepare corresponding composites. After thermal curing, BCB-functionalized phosphorus−oxygen flame-retardant resins are obtained. The results show that these thermosetting resins of POB_3 and M3 all showed good thermal stability, low total heat release (THR), and low CTE. Besides, they have a high elastic modulus and hardness and are expected to be used in the field of CCL substrates for electronic circuits.

2. EXPERIMENTAL SECTION

2.1. Materials. Diphenylphosphinic chloride (Ph_2POCl, 95%) was purchased from Shanghai Titan Technology Co., Ltd. (Shanghai, China). Phenylphosphonyl dichloride ($PhPOCl_2$, 98%) and phosphorus oxychloride ($POCl_3$, 98%) were both supplied by Infinity Scientific Co., Ltd. (Beijing, China). *n*-Butyl lithium (2.5 M) reagent was purchased from Shanghai Titan Technology Co., Ltd. (Shanghai, China). 4Br-BCB (95%) was supplied by Beichuan Ruihui Science and Technology Co., Ltd. (Mianyang, China). Tetraethoxysilane (97%) and tetramethoxysilane (TMOS, 97%) were purchased from J&K Scientific (China). BCBNPs were self-made in the laboratory.[33] Tetrahydrofuran (THF) was purchased from Beijing Bellwether Technology Co., Ltd. (Beijing, China) and was dried and freshly distilled under a nitrogen (N_2) atmosphere prior to use.

2.2. Measurements. ^{1}H NMR spectra were obtained using a Bruker AVANCE-400 instrument using deuterated chloroform as the solvent. Fourier transform infrared (FTIR) measurements at 400−4000 cm^{-1} were conducted on a Nicolet FTIR 5700 spectrophotometer at room temperature. High-resolution mass spectrum were obtained using a Thermo Scientific Q Exactive instrument. The ion source used is electrospray ionization, and the solvent is dichloromethane. On the SDT Q 600 synchronous thermogravimetric analyzer, thermogravimetric analysis (TGA) and differential scanning calorimetry (DSC) were performed at the rate of 10 °C/min in a N_2 atmosphere. Scanning electron microscopy (SEM) images were obtained using a ZEISS EVO 18 instrument. Microscale combustion calorimetry (MCC) analysis was performed using a FAA-PCFC instrument (Fire Testing Technology., Inc), using a high-precision MFC, with response time less than 0.1 s, ± 1% FS accuracy, and ASTM D7309-2007a as the test standard. These samples after vacuum drying were tested under a mixed flow atmosphere (80% N_2 and 20% O_2), with a heating rate of 1 °C/s, and from room temperature to 800 °C

https://doi.org/10.1021/acsomega.2c08159
ACS Omega 2023, 8, 9464−9474

Scheme 1. Synthesis Route of Monomers and Cured Resins

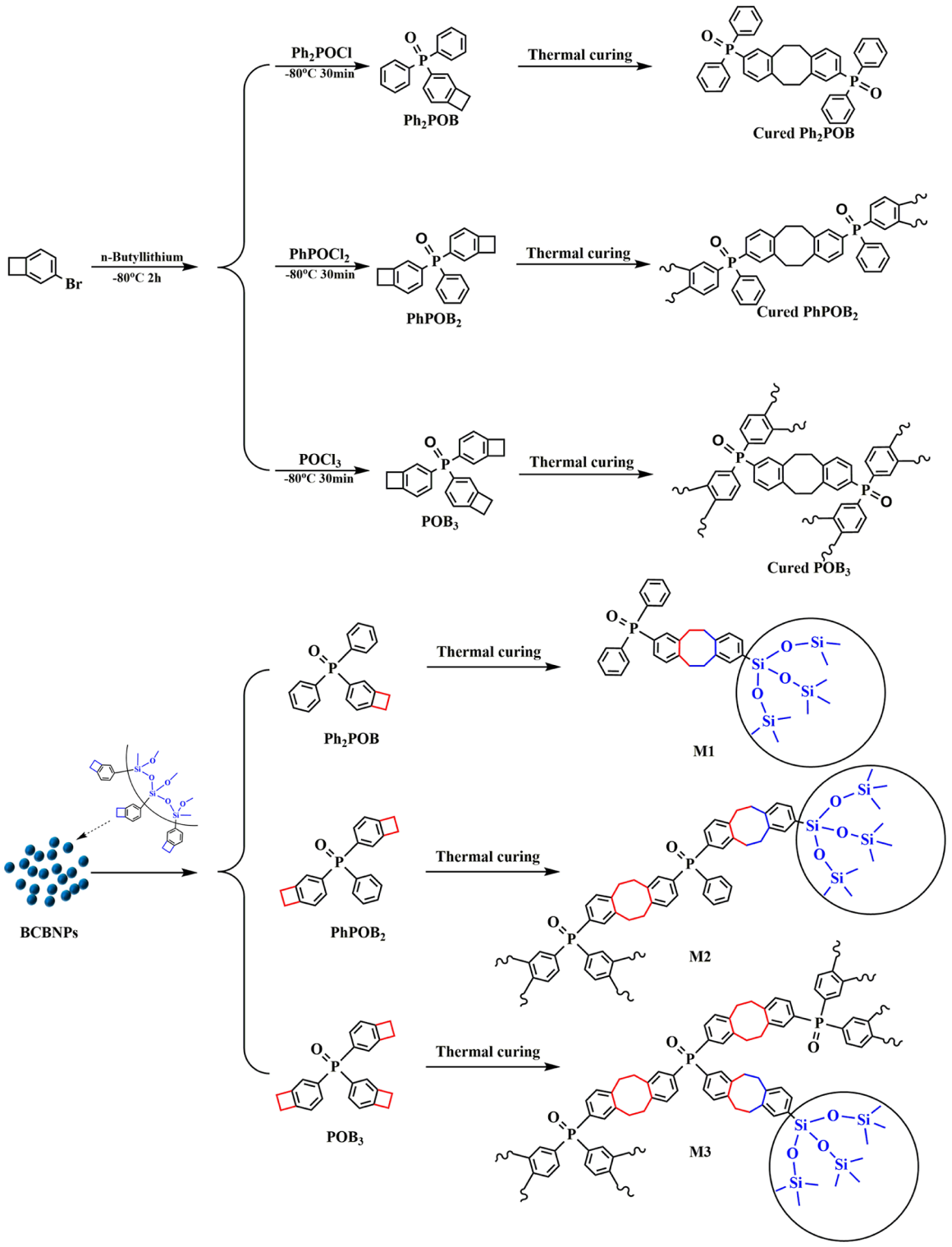

conditions. Raman spectra were obtained using a Renishaw inVia instrument to analyze the graphitization degree of residual carbon. Thermomechanical analysis (TMA) was performed using a USA-TA-Q400 instrument. These samples after vacuum drying were tested under a N_2 atmosphere, with the temperature rise rate of 5 °C/min, from room temperature to 300 °C (the temperature range of Ph_2POB and M1 is from room temperature to 200 °C). Nanoindentation was performed using an Agilent Nano Indenter G200 (U9820A, Agilent Technologies., Inc.) at room temperature. A strain rate of 0.2 s^{-1} was constantly maintained during the addition of the load until the indenter reached a depth of 2000 nm on the surface of the scaffold. The load was maintained at the maximum value for 10 s. To ensure the reliability of these nanoscale deformation measurements, at least five indents were performed on each sample to obtain effective data. The dielectric constant of the resins was measured on an Agilent 4294A impedance analyzer with varying frequencies at ambient

https://doi.org/10.1021/acsomega.2c08159
ACS Omega 2023, 8, 9464−9474

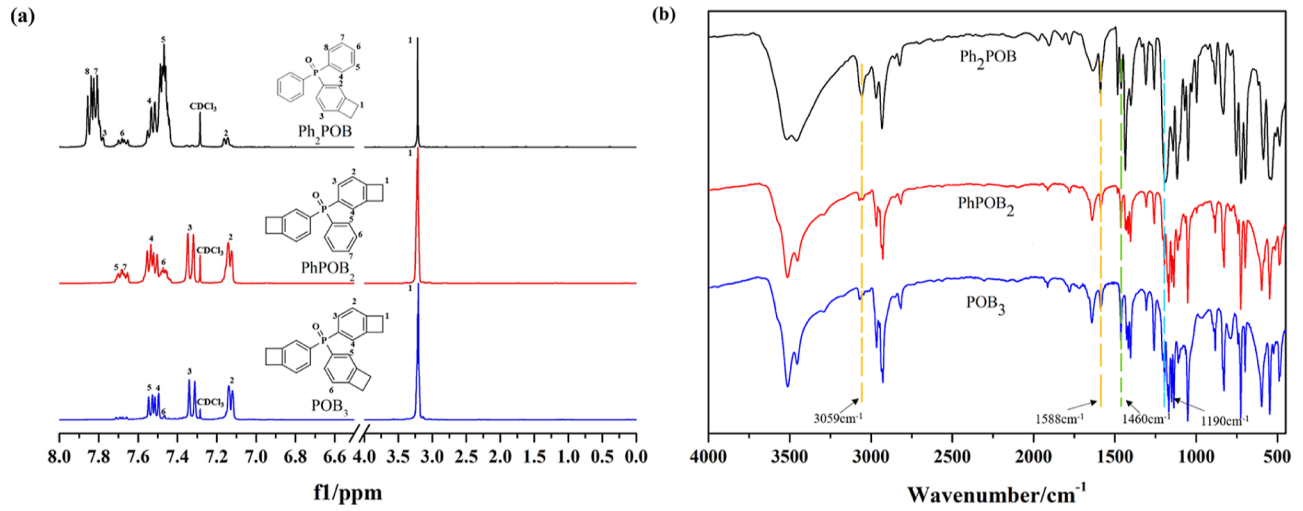

Figure 1. (a) ^{1}H NMR spectra of multi-BCB phosphine oxide monomers; (b) FTIR spectra of multi-BCB phosphorus oxide monomers.

temperatures (the 6.5 ± 0.05 mm diameter cylindrical samples were polished to a thickness of 3.0 ± 0.1 mm. After the samples were thoroughly dried under vacuum, gold was deposited via vacuum evaporation on both sides of the samples as electrodes). The dielectric constant was calculated using the following equation

$$\varepsilon_r = (C \times d)/(\varepsilon_0 \times S)$$

where C, d, and S denote the capacitance, thickness, and electrode area of the materials, respectively. ε_0 denotes the permittivity of free space and equals 8.854×10^{-12} F/m.

2.3.1. Synthesis of Ph_2POB, $PhPOB_2$, and POB_3. Three phosphorus oxide monomers with different amounts of BCB were synthesized (the synthetic route is shown in Scheme 1.) Take the synthesis of Ph_2POB as an example: in the early stage, the reaction devices were subjected to anhydrous and oxygen free treatment. 2.64 g (15 mmol) of 4Br-BCB and 40 mL of solvent dry THF were added to a 100 mL double-ended round-bottom flask equipped with magnetic stirring and a constant pressure dropping funnel, and then 1.0 g (15 mmol) of *n*-butyl lithium was slowly dripped through the constant pressure dropping funnel. After dropping, it was allowed to react at a low temperature of −80 °C for 2 h, and 3.8 g (16 mmol) of Ph_2POCl was slowly dropped through a constant pressure dropping funnel. After dropping, it was allowed to react at a low temperature of −80 °C for 30 min, and then it slowly rose to room temperature for another 48 h. After the reaction, anhydrous methanol was dropped to quench the unreacted *n*-butyl lithium, washed with UP water three times to remove impurities, and purified (volume ratio of ethyl acetate and petroleum ether is 1:4) through a chromatographic column (ethyl acetate recrystallized) to obtain white powders. The synthesis methods of Ph_2POB, $PhPOB_2$, and POB_3 are similar to that mentioned above, and the yields are 70, 64, and 61%, respectively.

The ^{1}H NMR spectra of the monomers are shown in Figure 1a.

^{1}H NMR of Ph_2POB (400 MHz, $CDCl_3$, δ, ppm): 7.85−7.83 (d, 2H), 7.82−7.80 (d, 2H), 7.80−7.76 (d, 1H), 7.71−7.64 (q, 2H), 7.55−7.51 (t, 2H), 7.50−7.45 (t, 2H), 7.16−7.14 (d, 2H), 3.19 (s, 4H). HRMS (ESI) m/z calcd for $C_{20}H_{18}OP^+$ $(M + H)^+$, 305.10898; found, 305.10904.

^{1}H NMR of $PhPOB_2$ (400 MHz, $CDCl_3$, δ, ppm): 7.72−7.67 (d, 2H), 7.66−7.64 (s, 1H), 7.58−7.50 (q, 2H), 7.49−7.44 (q, 2H), 7.30−7.36 (d, 2H), 7.17−7.10 (d, 2H), 3.30−3.10 (d, 8H). HRMS (ESI) m/z calcd for $C_{22}H_{20}OP^+$ $(M + H)^+$, 331.12463; found, 331.12515.

^{1}H NMR of POB_3 (400 MHz, $CDCl_3$, δ, ppm): 7.56−7.52 (d, 2H), 7.51−7.47 (d, 2H), 7.46 (s, 1H), 7.36−7.30 (d, 2H), 7.16−7.10 (d, 2H), 3.30−3.10 (d, 12H). HRMS (ESI) m/z calcd for $C_{24}H_{21}OPNa^+$ $(M + Na)^+$, 379.12222; found, 379.12228.

2.3.2. Preparation of Cured Resins. The thermal curing resins of the monomers is obtained by heating the white powder monomer in the curing mold to the molten state (100 °C) and holding it for 1 h before starting the curing process.

Some research works have shown that BCBNPs[33] (the synthetic method and route of BCBNPs, as shown in Supporting Information Scheme S1) can be added to BCB resins as fillers, which can improve the thermal stability of the resin and reduce the CTE of the resins by increasing the crosslinking point. Therefore, in this paper, we doped BCBNPs into the uncured monomers to prepare the corresponding composites M1, M2, and M3. BCBNPs were doped into each monomer at a mass ratio of 20%, heated to the molten state (100 °C), stirred vigorously for 1 h, then transferred to the curing mold, and cured to obtain the cured composites.

3. RESULTS AND DISCUSSION

3.1. Structural Characterization of Monomers. The FTIR of monomers is shown in Figure 1b, where 3059 cm^{-1} is the C−H stretching vibration absorption peak of the benzene ring, 1588 cm^{-1} is the vibration peak of the benzene ring skeleton absorption, and 1460 cm^{-1} is the bending vibration absorption peak of C−H of the BCB quaternion ring. At 1190 cm^{-1} is the strong stretching vibration absorption peak with P═O. At the same time, the three monomers were tested by HRMS (as shown in Supporting Information Figure S1). From the results, the molecular weights of the three monomers are consistent with the corresponding theoretical values.

The abovementioned monomers were characterized by ^{1}H NMR, FTIR, and HRMS. These results show that the synthesis of all monomers has been successful.

3.2. Thermal Curing Behavior Research. The cross-linking and curing behaviors of three monomers were studied

https://doi.org/10.1021/acsomega.2c08159
ACS Omega 2023, 8, 9464−9474

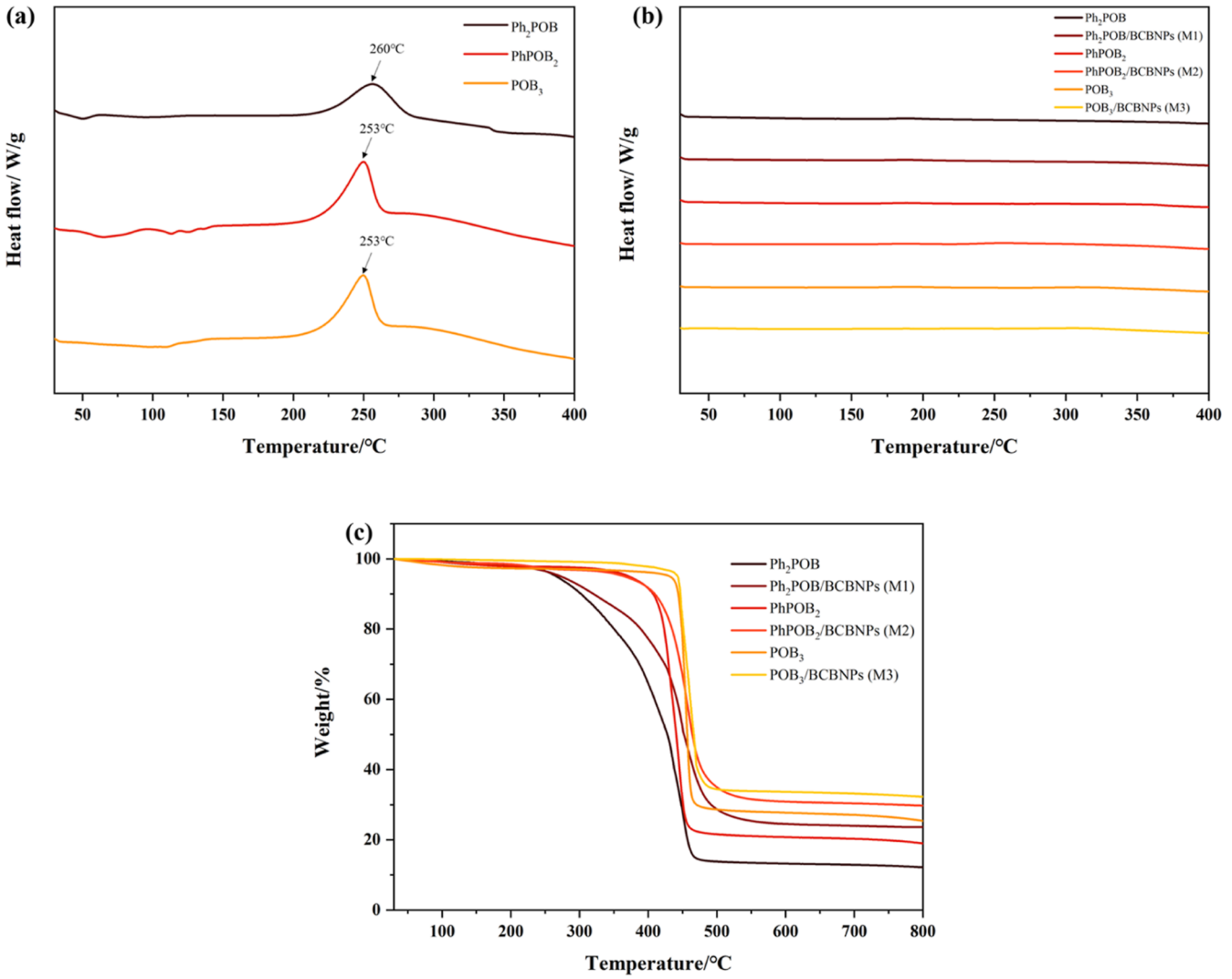

Figure 2. (a) DSC curves of multi-BCB phosphorus oxide monomers, (b) DSC curves of cured multi-BCB phosphorus oxide monomers and their composites, and (c) TGA curves of cured multi-BCB oxyphosphorous monomers and their composites.

by DSC, as shown in Figure 2a. As shown in the figure, all monomers show the exothermic peak of curing, and the initial temperature is 200 °C. For Ph_2POB, the maximum exothermic peak is 260 °C, which can be attributed to the reaction peak after the ring opening of BCB by heating. The end temperature is 290 °C, indicating that the ring opening reaction is basically over. $PhPOB_2$ and POB_3 show the maximum exothermic peak at 253 °C, and each shows a shoulder peak at about 280 °C. The shoulder peak of the monomer containing multiple BCB groups can be attributed to the further curing reaction of the cross-linked network structure formed by the initial partial polymerization.[34] At the same time, the end temperature of the ring opening reaction is delayed compared with that of Ph_2POB. This may be because the highly cross-linked network structure formed by the monomers containing multiple BCB groups requires a higher temperature to fully cure.

3.3. Thermal Stability Research. According to TGA, $PhPOB_2$, and POB_3 thermosetting resins show good thermal stability (as shown in Figure 2c). From the curve in the figure, we can see that Ph_2POB decomposes first with the increase of temperature (T_{d5} = 267 °C), which can be attributed to the limited cross-linking behavior of a single BCB group, which improves the thermal stability of OPFRs. However, with the increase of BCB groups in $PhPOB_2$ and POB_3 thermosetting resins, the crosslinking density increases, and the thermal stability has been significantly improved. The T_{d5} of $PhPOB_2$ is 372 °C and the T_{d5} of POB_3 is 431 °C are much higher than the T_{d5} of Ph_2POB, which greatly improves the thermal stability of traditional OPFRs materials.

Compared with the cured resins of monomers, the T_{d5} of their composite material is improved to a certain extent, but its carbon residue rate has been significantly increased to 23.6, 29.7, and 32.3% respectively. Figure 2b shows that there is no exothermic peak in the cured resin DSC curve, indicating that these BCB groups containing monomers and their composites have been completely cured under the set conditions, which confirms the thermal curing behavior of the monomers in Figure 2a. It shows high thermal stability, which can be attributed to the doping of BCBNPs, which not only improve the crosslinking density by cross-linking with monomers during the thermal curing process but also introduce the Si−O structure. The Si−O bond energy is relatively high, which makes it relatively stable and not easy to break. With BCBNPs are doped, it shows the synergistic thermal stability of P and Si,[35,36] which improve the both of thermal stability and carbon residue rate.

https://doi.org/10.1021/acsomega.2c08159
ACS Omega 2023, 8, 9464−9474

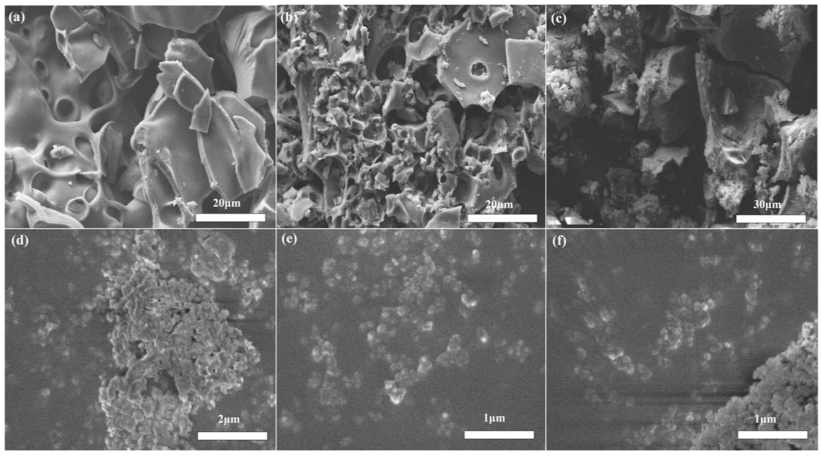

Figure 3. (a) SEM image of cured Ph_2POB Carbonization at 500 °C, (b) SEM image of cured $PhPOB_2$ carbonization at 500 °C, (c) SEM image of cured POB_3 carbonization at 500 °C, (d) SEM image of cured M1 carbonization at 800 °C, (e) SEM image of cured M2 carbonization at 800 °C, and (f) SEM image of cured M3 carbonization at 800 °C.

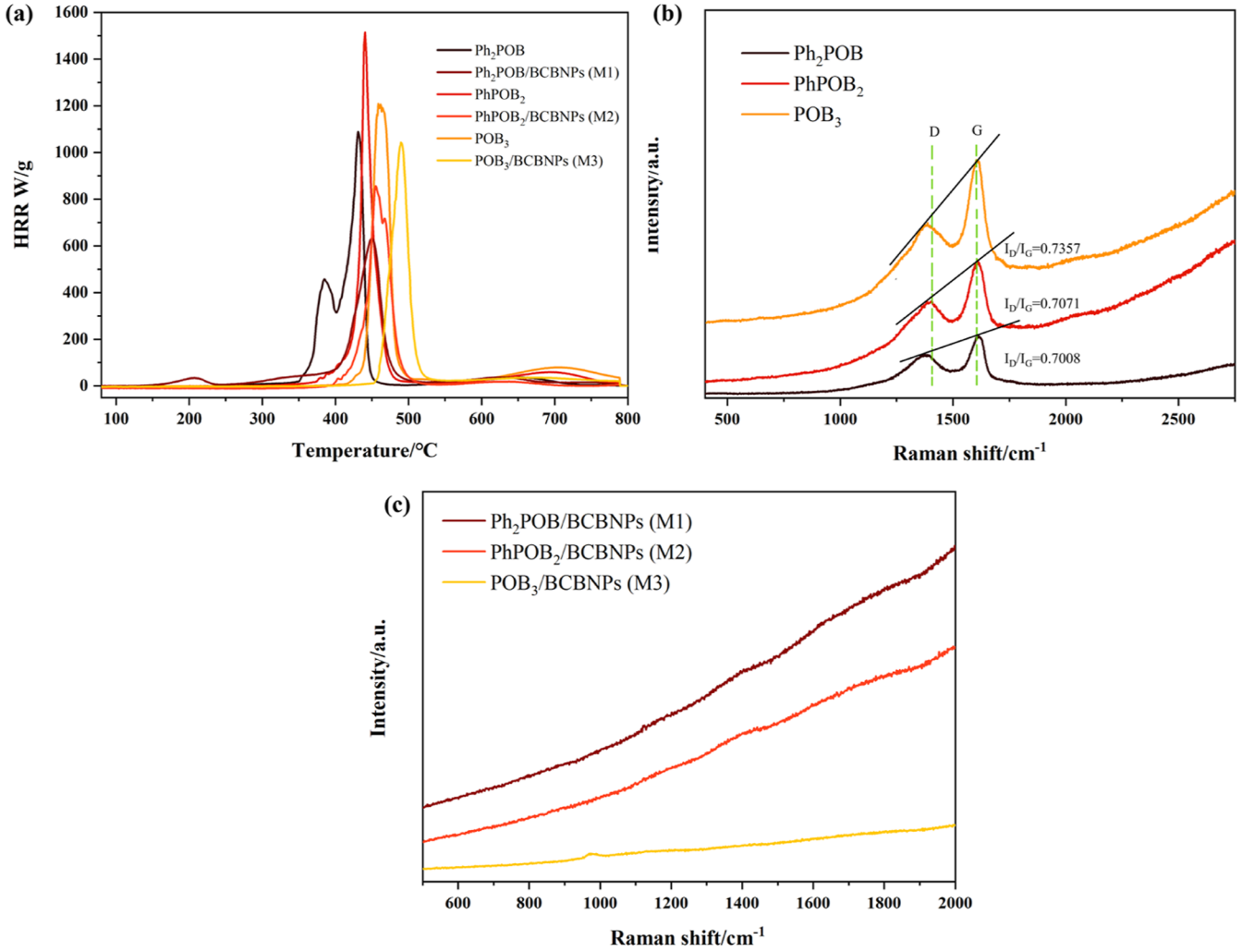

Figure 4. (a) MCC curves of cured multi-BCB oxyphosphorous monomers and their composites, (b) Raman spectra of cured multi-BCB phosphorus oxide monomers after carbonization at 500 °C, and (c) Raman spectra of cured composites after carbonization at 800 °C.

3.4. Morphology after Carbonization Research. The morphology of the cured monomers after carbonization at 500 °C is shown in Figure 3a−c. These cured monomers, Ph_2POB, $PhPOB_2$, and POB_3, show scaly residual carbon after carbonization at 500 °C, which can be attributed to the fact that P═O in the structure can promote carbon formation when decomposing at high temperature, and the cross-linking structure formed by the opening of the BCB group ring of the

https://doi.org/10.1021/acsomega.2c08159
ACS Omega 2023, 8, 9464−9474

monomer itself is also conducive to promoting carbon formation.

After carbonization at 800 °C (air atmosphere, hold for 1 h), the three cured monomers were basically decomposed, and there was basically no residue in the crucible. The morphology of the composites after carbonization at 800 °C is shown in Figure 3d−f. Due to being doped with BCBNPs, more complete spherical silicon nanoparticles were preserved after carbonization at 800 °C, which had a higher carbon residue rate and showed good flame retardancy.

3.5. Flame Retardancy Research. In order to test the combustion performance and heat release capacity of cured monomers and their composites, micro combustion calorimetry (MCC) was conducted. The test curve is shown in Figure 4a, and the relevant data are recorded in Table 1.

Table 1. MCC Data of Cured Multi-BCB Phosphorous Oxide Monomers and Their Composites

sample	HRC[a] (J/g K)	PHRR[b] (W/g)	THR[c] (kJ/g)	T_{PHRR}[d] (°C)	T_{TPHRR}[e] (s)
Ph_2POB	772.00	1091.00	29.60	430.90	282.00
$PhPOB_2$	1109.00	1521.00	29.80	439.80	309.50
POB_3	860.00	1166.00	30.50	456.90	319.50
M1	465.00	631.60	25.50	450.40	303.50
M2	607.00	859.60	23.40	455.30	321.00
M3	738.00	1043.60	23.10	489.70	341.50

[a]HRC represents the heat release capacity. [b]PHRR represents the peak HRR of the material. [c]THR represents the THR of the material. [d]T_{PHRR} represents the temperature at which the material reaches the peak HRR. [e]T_{TPHRR} represents the time when the measured material reaches the peak HRR.

It is shown from the figure and the table that the sharp peak of the heat release rate (HRR) curve of monomers Ph_2POB, $PhPOB_2$, and POB_3 gradually delayed, which indicates that $PhPOB_2$ and POB_3 have a higher heat release temperature. Meanwhile, the T_{PHRR} for Ph_2POB, $PhPOB_2$, and POB_3 were gradually increased, and the T_{TPHRR} was increased as well. Besides, the THR of these cured monomers does not show much difference. The T_{PHRR} of these thermosetting resins gradually increased means that they need higher temperatures to reach the maximum HRR. In addition, the T_{TPHRR} gradually increased, which also confirms that these thermosetting resins need more time to be decomposed, which showed good flame retardancy. It is can be attributed to the fact that P═O in the cured monomers make the molecular structure more stable and are not easy to be damaged at higher temperatures. Moreover, the high-density network structure formed after BCB groups crosslinking also ensures the thermal stability of these thermosetting resins and their good flame retardancy.

Compared with the cured monomers, the THR of these composites M1, M2, and M3 showed a significant decrease, indicating a lower THR. At the same time, T_{PHRR} and T_{TPHRR} of M1, M2, and M3 also showed a certain increase compared with cured monomers. It can be attributed to the fact that doped with BCBNPs not only introduce more BCB groups, which further improves the crosslinking density, but also introduce Si−O bonds with higher bond energies, which are relatively stable at high temperatures and are not easy to be destroyed. Furthermore, these composites form a good protective carbon layer in the process of ignition and initial combustion, blocking the exchange of heat and materials, and the P in the cured resin releases phosphorus-containing free radicals during combustion, such as $PO^{\cdot}$ and $PO_2^{\cdot}$.[37] These free radicals can be used as effective free radical scavengers to inhibit the gas-phase chain propagation reaction during combustion (possible flame retardant mechanisms are as follows). The highly cross-linked network structure, Si═O bond and P═O bond together make these thermosetting resins have high thermal stability and flame retardancy. They play a synergistic role in the flame retardancy of P and Si, which showed good flame retardancy.[38,39]

$$\dot{O}H + \dot{P}O \rightleftharpoons HO - \dot{P} = O$$

$$\dot{H} + \dot{P}HO_2 \rightleftharpoons HO - \dot{P} = O$$

$$\dot{O}H + \dot{P}HO_2 \rightleftharpoons HO\dot{P} = O_2$$

Raman spectrum testing is usually used to analyze the degree of graphitization of carbon residue after combustion of polymer materials. The smaller the ratio of the characteristic peaks D and G of atomic crystals, the higher the degree of graphitization, the smaller the lattice defects, and the smoother and denser the surface of carbon residue. As shown in Figure 4b, after carbonization at 500 °C in air atmosphere, the I_D/I_G value of cured monomers increases with the increase of BCB groups.

However, the composite materials doped with BCBNPs did not show an obvious Raman spectrum signal after carbonization at 800 °C in air atmosphere (as shown in Figure 4c). It can be considered that the elements P, C, and H contained in the composite are basically completely decomposed under this condition, and the remaining carbon is basically spherical silicon nanoparticles. That is, the combustion residual carbon of the composites added with BCBNPs has smaller micro size, which is also confirmed by the existence of nanosilicon spheres in the SEM image (as shown in Figure 3d−f), which can be attributed to the presence of silicon containing components in the composites. Generally, the smaller the size of the residual carbon, the higher the thermal shielding efficiency. Therefore, doped with BCBNPs can obtain better flame retardancy.

3.6. CTE Research. Their thermal mechanical properties and CTE are tested by thermal mechanical analysis (TMA), as shown in Figure 5. The curves show that in the temperature range from room temperature to 300 °C (CTE of Ph_2POB and

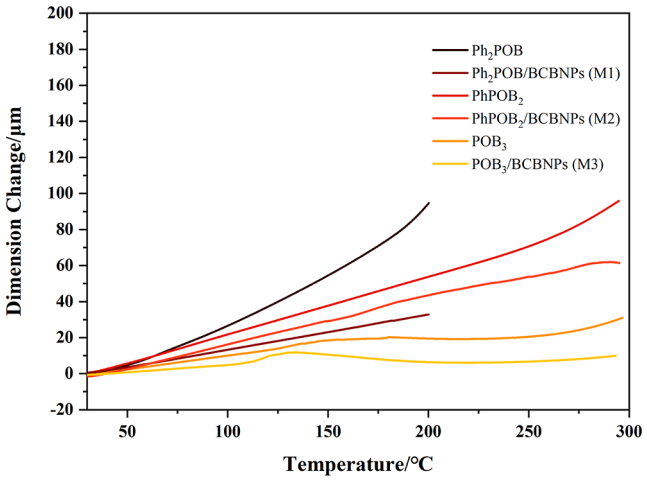

Figure 5. TMA curves of cured multi-BCB oxyphosphorous monomers and their composites.

https://doi.org/10.1021/acsomega.2c08159
ACS Omega 2023, 8, 9464−9474

M1 are obtained at room temperature to 200 °C), the curves of cured resins are gradually flattened with the rise of temperature. The CTE of the cured resins can be calculated from the TMA curve in Figure 5, and the results are shown in Table 2. The results show that the CTE of cured monomers of

Table 2. T_{d5}, THR, CTE, Elastic Modulus, Hardness, and k Data of Cured Multi-BCB Phosphorus Oxide Monomers and Their Composites

sample	T_{d5} (°C)	THR (kJ/g)	CTE[a] (ppm/°C)	elastic modulus (GPa)	hardness (GPa)	k
Ph_2POB	267	29.60	118.40	4.35	0.24	2.85
$PhPOB_2$	372	29.80	74.60	4.82	0.29	2.76
POB_3	431	30.50	23.57	6.20	0.39	3.47
M1	273	25.50	46.96	6.75	0.34	3.09
M2	365	23.40	56.92	6.80	0.37	3.21
M3	443	23.10	16.71	10.03	0.83	3.52

[a]CTE of Ph_2POB and M1 are obtained at room temperature to 200 °C.

Ph_2POB, $PhPOB_2$, and POB_3 decreased gradually. According to the calculation results, the CTE of POB_3 is as low as 23.71 ppm/°C. The low CTE of POB_3 can be attributed to the increase of BCB groups in the monomers, which increase the degree of crosslinking and form a more intensive cross-linking network structure.

These composite materials are doped with BCBNPs that take effect to reduce the CTE of cured monomers of Ph_2POB, $PhPOB_2$, and POB_3. Compared with the monomers, the CTE of the M1 and M2 composites decreased to 46.96 and 56.92 ppm/°C, respectively. Especially M3 shows very low CTE, reaching as low as 16.71 ppm/°C, much lower than the previously reported CTE.[40,41] The low CTE can be attributed to the BCBNPs being doped. By introducing more BCB groups, these thermosetting resins form a network structure with a higher crosslinking degree. In addition, the P═O bond and the Si−O bond in the composites have large bond energies, which increases the intermolecular force. In these thermosetting resins, during the heating process, the relative movement between molecules is more difficult, which will affect the displacement between polymer molecules and make them not easy to deform. These thermosetting resins have stable properties at higher temperatures, are not easy to deform, and can be processed, which is conducive to the preparation of relevant electronic circuit copper clad plate materials.[19]

3.7. Mechanical Properties' Research. The mechanical properties of cured monomers and their composites were tested by nanoindentation technology, as shown in Table S1. The results show that the elastic modulus and hardness of cured resins show a trend of gradual increase, which can be attributed to the higher degree of crosslinking and curing with the increase of BCB groups in monomers, and the high crosslinked network structure formed gives higher elastic modulus and hardness. The average elastic modulus and hardness of the cured resin were 4.3−6.2 GPa and 0.2−0.4 GPa, respectively. Especially, POB_3 has a higher elastic modulus (6.20 GPa) and a higher hardness (0.39 GPa), which can be attributed to the higher crosslinking density of the three BCB groups in its structure after thermal curing.

With more BCBNPs being doped, more BCB groups are provided, which also means that there will be more cross-linking sites and a higher cross-linking density after thermal curing. All composites also show similar laws. The results also show that the corresponding elastic modulus and hardness were significantly increased compared with the monomers, especially the elastic modulus and hardness of M3 reached 10.03 GPa and 0.83 GPa respectively, showing good mechanical properties.

Besides, with the increase of indentation depth, the elastic modulus and hardness of most cured monomers and their composites are not constant but increase gradually with the decrease of load (indenter displacement) within a certain range (as shown in Figure S2a,b). This phenomenon, called the size effect of nanoindentation, can be explained by the strain gradient plasticity theory developed based on the molecular kinking mechanism.[42,43] Its size effect is mainly caused by size-related deformation. The degree of size-dependent deformation is affected by the bending stiffness, molecular weight, crosslinking density, and flexibility of the polymer molecular chain. The larger the molecular weight, the stronger the indentation size effect. At the same time, the higher the crosslinking density, the higher the specific strain gradient modulus, and the lower the yield kink density. When the indentation depth is greater than 1500 nm, the nanosize effect tends to be stable. At this time, the elastic modulus and hardness value basically remain unchanged, which can be attributed to the fact that the molecular chain relaxation ability matches the indentation rate with the increase of the indentation depth and its modulus and hardness reach a fixed value. Compared with other thermosetting resins, M3, with its higher elastic modulus and hardness, has a relatively large degree of reduction (as shown in Figure S2c), which can be attributed to its higher molecular weight. The elastic modulus and hardness of M3 are as high as 10.03 and 0.83 GPa, respectively, which are much higher than those of PCOS cured resin (1.84 and 0.21 GPa).[44] The abovementioned results show that M3 thermosetting resin with high dimensional stability and mechanical properties is expected to be used in the field of the CCL substrate for microelectronic circuits.

3.8. Dielectric Properties' Research. Meanwhile, we also conducted relevant dielectric performance tests. The frequency correlation curve of the relative dielectric constant (k) of these thermosetting resins at room temperature is shown in Figure S3, and the relative dielectric constant is shown in Table 2. The k values of cured Ph_2POB, $PhPOB_2$, and POB_3, and their composites M1, M2, and M3 are not stable. Both of Ph_2POB and $PhPOB_2$ monomers show relatively low dielectric constants, which may be due to the fact that the eight membered ring or ethylene chain generated by dimerization or polymerization of the BCB groups ring is used as spacer group to prevent the formation of π bond molecular delocalization so that they have a low k value. However, although POB_3 and composite materials M1, M2, and M3 have the most BCB groups, it can be seen from the figure that an increase of BCB groups does not necessarily mean a lower dielectric constant. When BCBNPs are doped, the dielectric constant increases, which may be attributed to the excessive BCB groups in POB_3 and M1, M2, and M3. After thermal curing, a highly cross-linked network structure is generated inside. Although high crosslinking density brings high thermal stability and flame retardance. However, the excessive crosslinking density will

https://doi.org/10.1021/acsomega.2c08159
ACS Omega 2023, 8, 9464−9474

lead to a decrease of free volume but a increase of the dielectric constant.[47] Compared with the dielectric constant of traditional CCL substrate materials, such as HBP (k: 4.29/10^7 Hz),[1] rPPO/CE (k: 3.85/10^7 Hz),[45] and rPPO/CP (k: 3.76/10^7 Hz),[46] are still lower. The comparison between cured resin M3 and the traditional CCL substrate is shown in Figure 6 and

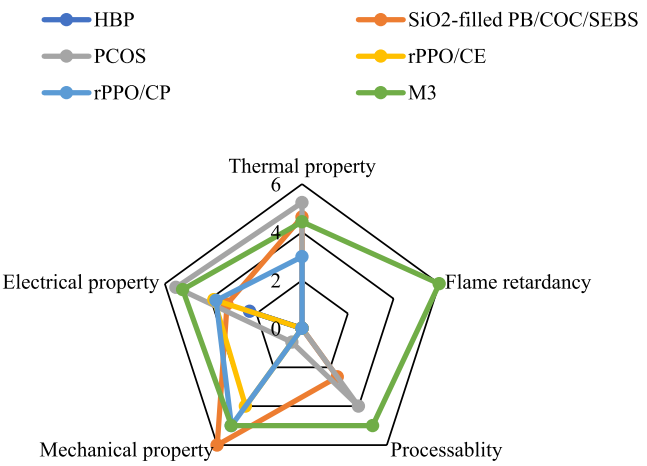

Figure 6. Comparison of cured resin M3 with traditional CCL substrate materials.

Table 3. Compared with traditional CCL substrate materials, M3 has higher thermal stability, lower CTE, better mechanical properties, and a relatively lower dielectric constant. The most important thing is that M3 itself has flame retardancy, which can be achieved without adding other additional flame retardants. These comprehensive properties make M3 hopeful to be used in the field of the CCL substrate for electronic circuits.

4. CONCLUSIONS

Multi-BCB oxyphosphorous monomers were synthesized, and highly crosslinked thermosetting resins with good thermal stability, flame retardancy, low CTE, and mechanical properties were obtained. Moreover, these monomers were mixed with BCBNPs and cured to obtain their corresponding composites. These composites not only have better thermal stability and flame retardancy but also have lower CTE. It is shown that the more BCB groups on the phosphorus oxide monomers, the higher its crosslinking structure, which helps to improve its thermal stability, flame retardancy, and carbon residue rate. These composites corresponding to its monomers show a lower THR (the THR of M3 is 23.1 kJ/g) due to the synergistic flame retardancy of P and Si. The cured POB_3 and M3 show good thermal stability (T_{d5} = 431 °C and T_{d5} = 443 °C) and flame retardancy. These cured resins show good mechanical properties as well, especially the elastic modulus and hardness of M3, which are up to 10.03 and 0.83 GPa, respectively. These thermosetting resins also show good dielectric properties. The dielectric constants of the monomers Ph_2POB and $PhPOB_2$ are lower than 2.85, which make the OPFRs materials also have low dielectric properties. These thermosetting flame retardant resins can achieve good flame retardancy without adding additional flame retardants and are expected to be used in high-performance CCL composite resin matrix and related electronic packaging materials due to their high thermal stability, good flame retardancy, low CTE, good mechanical properties, and low dielectric constant.

■ ASSOCIATED CONTENT

Supporting Information

The Supporting Information is available free of charge at https://pubs.acs.org/doi/10.1021/acsomega.2c08159.

High-resolution mass spectrum, elastic modulus and hardness values, cured multi-BCB phosphorus oxide monomers and their composites, and frequency correlation curves of the cured relative dielectric constant (k) of multi-BCB oxyphosphorous monomers and their composites (PDF)

■ AUTHOR INFORMATION

Corresponding Authors

Jiajun Ma − *School of Materials and Chemistry and State Key Laboratory of Environmentally-friendly Energy Materials, Southwest University of Science and Technology, Mianyang 621010, China;* orcid.org/0000-0002-1384-1445; Email: jiajunma@yeah.net

Xu Ye − *School of Materials and Chemistry and School of Continuing Education, Southwest University of Science and Technology, Mianyang 621010, China;* orcid.org/0000-0003-3399-5799; Email: yexu@swust.edu.cn

Authors

Chao Guo − *School of Materials and Chemistry and State Key Laboratory of Environmentally-friendly Energy Materials, Southwest University of Science and Technology, Mianyang 621010, China*

Qiuxia Peng − *School of Materials Science and Engineering, Sichuan University of Science & Engineering, Zigong 643000, China;* orcid.org/0000-0002-1627-0027

Hubo Wei − *School of Materials and Chemistry and State Key Laboratory of Environmentally-friendly Energy Materials, Southwest University of Science and Technology, Mianyang 621010, China*

Jiaying Liu − *School of Materials and Chemistry and State Key Laboratory of Environmentally-friendly Energy Materials, Southwest University of Science and Technology, Mianyang 621010, China*

Table 3. Comparison of Cured Resin M3 with Traditional CCL Substrate Materials

materials	T_{d5} (°C)	THR (kJ/g)	CTE (ppm/°C)	elastic modulus (GPa)	k	reference
HBP					4.29	1
SiO_2-filled PB/COC/SEBS	463		24.98		3.28	19
PCOS	523		79	1.71	2.51	41
rPPO/CE					3.85	45
rPPO/CP	298				3.76	46
M3	443	23.1	16.71	10.03	3.52	

https://doi.org/10.1021/acsomega.2c08159
ACS Omega 2023, 8, 9464−9474

Xinyu Hu − *School of Materials and Chemistry and State Key Laboratory of Environmentally-friendly Energy Materials, Southwest University of Science and Technology, Mianyang 621010, China*

Juan Peng − *School of Materials and Chemistry and State Key Laboratory of Environmentally-friendly Energy Materials, Southwest University of Science and Technology, Mianyang 621010, China*

Junxiao Yang − *School of Materials and Chemistry and State Key Laboratory of Environmentally-friendly Energy Materials, Southwest University of Science and Technology, Mianyang 621010, China*

Complete contact information is available at: https://pubs.acs.org/10.1021/acsomega.2c08159

Notes

The authors declare no competing financial interest.

■ ACKNOWLEDGMENTS

This work was financially supported by the Sichuan Natural Science Foundation (no. 2022NSFSC0032) and the Open Fund of State Key Laboratory of Environment-Friendly Energy Materials, Southwest University of Science and Technology (no. 21fksy03 and no. 20fksy03).

■ REFERENCES

(1) Shi, J. H.; Zhang, X. R.; Weng, L.; Zhu, X. S.; Liu, L. Z. Study on low dielectric laminate modified by hyperbranched polyester of caprylic acid and hexanoic acid co-blocking. *J. Mater. Sci. Mater. Electron.* **2020**, *31*, 5068−5076.

(2) Kim, Y. H.; Lim, Y. W.; Kim, Y. H.; Bae, B. S. Thermally Stable Siloxane Hybrid Matrix with Low Dielectric Loss for Copper-Clad Laminates for High-Frequency Applications. *ACS Appl. Mater. Interfaces* **2016**, *8*, 8335−8340.

(3) Zhao, X.-Y.; Liu, H. J. Review of polymer materials with low dielectric constant. *Polym. Int.* **2010**, *59*, 597−606.

(4) Zhang, S.; Li, X. D.; Fan, H. J.; Fu, Q.; Gu, Y. Epoxy nanocomposites: Improved thermal and dielectric properties by benzoxazinyl modified polyhedral oligomeric silsesquioxane. *Mater. Chem. Phys.* **2019**, *223*, 260−267.

(5) Gu, X.; Zhang, Z. J.; Yuan, L.; Liang, G. Z.; Gu, A. J. Developing high performance cyanate ester resin with significantly reduced postcuring temperature while improved toughness, rigidity, thermal and dielectric properties based on manganese-Schiff base hybridized graphene oxide. *Chem. Eng. J.* **2016**, *298*, 214−224.

(6) Zhi, M. Y.; Yang, X.; Fan, R.; Yue, S.; Zheng, L. L.; Liu, Q. Y.; He, Y. H. A comprehensive review of reactive flame-retardant epoxy resin: fundamentals, recent developments, and perspectives. *Polym. Degrad. Stabil.* **2022**, *201*, 109976.

(7) Ai, Y. F.; Liu, X. D.; Bai, W. B.; Lin, Y. C.; Xie, R. R.; Jian, R. K. From herbicide to flame retardant: The lamellar-like phosphorus-bridged amitrole toward high fire safety epoxy resin with light smoke and low toxicity. *Chemosphere* **2022**, *291*, 132704.

(8) Bruchajzer, E.; Frydrych, B.; Szymańska, J. A. Organophosphorus flame retardants-Toxicity and influence on human health. *Med. Pr.* **2015**, *66*, 235−64.

(9) Wendels, S.; Chavez, T.; Bonnet, M.; Salmeia, K. A.; Gaan, S. Recent Developments in Organophosphorus Flame Retardants Containing P-C Bond and Their Applications. *Materials* **2017**, *10*, 784.

(10) Du, J.; Li, H. X.; Xu, Q. W.; Zhou, M. Q.; Jin, J. H.; Tang, J. A review of organophosphorus flame retardants (OPFRs): occurrence, bioaccumulation, toxicity, and organism exposure. *Environ. Sci. Pollut. Res.* **2019**, *26*, 22126−22136.

(11) Shen, M. Y.; Kuan, C. F.; Kuan, H. C.; Ke, C. Y.; Chiang, C. L. Flame Retardance and Char Analysis of an Eco-Friendly Polyurethane Hyperbranched Hybrid Using the Sol-Gel Method. *Sustainability* **2021**, *13*, 486.

(12) Huang, R.; Guo, X. Y.; Ma, S. Y.; Xie, J. X.; Xu, J. Z.; Ma, J. Novel Phosphorus-Nitrogen-Containing Ionic Liquid Modified Metal-Organic Framework as an Effective Flame Retardant for Epoxy Resin. *Polymers* **2020**, *12*, 108.

(13) Chen, Z. W.; Guo, Y.; Chu, Y. P.; Chen, T. T.; Zhang, Q. W.; Li, C. X.; Jiang, J. C.; Chen, T.; Yu, Y.; Liu, L. X. Solvent-free and electron transfer-induced phosphorus and nitrogen-containing hetero-structures for multifunctional epoxy resin. *Compos. B Eng.* **2022**, *240*, 109999.

(14) Niu, M.; Zhang, Z. Z.; Wei, Z. Z.; Wang, W. J. Effect of a Novel Flame Retardant on the Mechanical, Thermal and Combustion Properties of Poly (Lactic Acid). *Polymers* **2020**, *12*, 2407.

(15) Hu, Z. D.; Liu, X. Q.; Ren, T. L.; Saeed, H. A. M.; Wang, Q.; Cui, X.; Huai, K.; Huang, S. H.; Xia, Y. M.; Fu, K.; et al. Research progress of low dielectric constant polymer materials. *J. Polym. Eng.* **2022**, *42*, 677−687.

(16) Lee, C.; Kim, S.; Jo, M.; Lee, J. Residual Interfacial Deformation in Flexible Copper Clad Laminate Occurring During Roll-to-Roll Composite Film Manufacturing. *Int. J. Precis Eng. Manuf. Green Energy* **2021**, *8*, 805−815.

(17) Liu, T. J.; Sil, M. C.; Chen, C. M. Well-organized organosilane composites for adhesion enhancement of heterojunctions. *Compos. Sci. Technol.* **2020**, *193*, 108135.

(18) Kim, S.; Wang, X. Y.; Ando, S.; Wang, X. G. Hybrid ternary composites of hyperbranched and linear polyimides with SiO2: a research for low dielectric constant and optimized properties. *RSC Adv.* **2014**, *4*, 42737−42746.

(19) Dong, J. J.; Wang, H.; Zhang, Q. L.; Yang, H.; Cheng, J. L.; Xia, Z. Y. Hydrocarbon Resin-Based Composites with Low Thermal Expansion Coefficient and Dielectric Loss for High-Frequency Copper Clad Laminates. *Polymers* **2022**, *14*, 2200.

(20) Chen, B. W.; Ding, Q.; Ni, D. W.; Wang, H. D.; Ding, Y. S.; Zhang, X. Y.; Dong, S. M. Microstructure and mechanical properties of 3D Cf/SiBCN composites fabricated by polymer infiltration and pyrolysis. *J. Adv. Ceram.* **2021**, *10*, 28−38.

(21) Momenzadeh, N.; Miyanaji, H.; Berfield, T. A. Influences of zirconium tungstate additives on characteristics of polyvinylidene fluoride (PVDF) components fabricated via material extrusion additive manufacturing process. *Int. J. Adv. Manuf. Technol.* **2019**, *103*, 4713−4720.

(22) Liu, G. W.; Zhang, Y. W.; Thomas, M. P.; Ullah, A.; Pharr, M.; Guiton, B. S.; Banerjee, S. Negative Thermal Expansion HfV2O7 Nanostructures for Alleviation of Thermal Stress in Nanocomposite Coatings. *ACS Appl. Mater. Interfaces* **2021**, *13*, 44723−44732.

(23) Chun, H.; Park, S. Y.; Park, S. J.; Kim, Y. J. Preparation of low-CTE composite using new alkoxysilyl-functionalized bisphenol A novolac epoxy and its CTE enhancement mechanism. *Polymer* **2020**, *207*, 122916.

(24) Wu, B.; Mao, X.; Wang, C. Y.; Deng, T.; Li, R.; Xu, Y.; Tang, X. H. Different Organic Peroxides that Cure Low- k 1, 2-PB / SBS / EPDM Composites for High-Frequency Substrate. *J. Vinyl Addit. Technol.* **2020**, *26*, 524−535.

(25) Hassan, M. M.; Takahashi, T.; Koyama, K. Thermal stability, mechanical properties, impact strength, and uniaxial extensional rheology of reactive blends of PS and SBS polymers. *Polym. Bull.* **2019**, *76*, 5537−5557.

(26) Nair, A. B.; Kalappura, U. G.; Kurian, P.; Joseph, R. Dielectric behavior of aluminum hydroxide-filled oil-extended ethylene-propylene-diene-monomer rubber composites in microwave fields. *Polym. Eng. Sci.* **2013**, *53*, 699−706.

(27) Kotha, S.; Lahiri, K.; Tangella, Y. Recent Advances in Benzocyclobutene Chemistry. *Asian J. Org. Chem.* **2021**, *10*, 3166−3185.

(28) Gies, A. P.; Spencer, L.; Rau, N. J.; Boopalachandran, P.; Rickard, M. A.; Kearns, K. L.; McDougal, N. T. Thermally Induced Cross-Linking and Degradation Reactions of Benzocyclobutene-Based Polymers. *Macromolecules* **2017**, *50*, 2304−2319.

(29) Cheng, Y. R.; Qi, T. K.; Jin, Y. X.; Deng, D. Y.; Xiao, F. Highly cross-linked thermosetting resin of maleimidobenzoxazine functionalized with benzocyclobutene. *Polymer* **2013**, *54*, 143−147.
(30) Huang, Y. W.; Zhang, S. B.; Hu, H.; Wei, X. N.; Yu, H. T.; Yang, J. X. Synthesis of poly(silmethylene)s via ring-opening polymerization of benzocyclobutene functionalized disilacyclobutene and their low-dielectric and thermal properties. *Polym. Adv. Technol.* **2017**, *28*, 1480−1488.
(31) Li, X.; Zhong, N.; Hu, H.; Zhang, Y. F.; Huang, Y. W.; Ye, X.; Yang, J. X. Preparation and Properties of Low Dielectric Constant Siloxane/Carbosilane Hybrid Benzocyclobutene Resin Composites. *Materials* **2021**, *14*, 6548.
(32) Cheng, Y. R.; Cai, J.; Li, J. Y.; Wu, X. L.; Shi, Y. F.; Wang, J. Multibenzocyclobutene Functionalized Silane for Low-k Polyarylsilane Thermosets with Low Coefficient of Thermal Expansion and High Thermostability. *ACS Appl. Polym. Mater.* **2019**, *1*, 2622−2626.
(33) Peng, Q. X.; Hu, H.; Ma, J. J.; Yang, J. X. High performance low dielectric polybenzocyclobutene nanocomposites with organic-inorganic hybrid silicon nanoparticles. *Phys. Chem. Chem. Phys.* **2022**, *24*, 6570−6579.
(34) Nava, P.; Carissan, Y. On the ring-opening of substituted cyclobutene to benzocyclobutene: analysis of π delocalization, hyperconjugation, and ring strain. *Phys. Chem. Chem. Phys.* **2014**, *16*, 16196−16203.
(35) Liu, J.; Kong, D. Z.; Dong, C. H.; Zhang, Z.; Wang, S.; Sun, H.; Lu, Z. Preparation of a novel P/Si polymer and its synergistic flame retardant application on cotton fabric. *Cellulose* **2021**, *28*, 8735−8749.
(36) Chen, L. M.; Zeng, S. H.; Xu, Y.; Nie, W. Y.; Zhou, Y. F.; Chen, P. P. Epoxy-modified silicone resin based N/P/Si synergistic flame-retardant coating for wood surface. *Prog. Org. Coat.* **2022**, *170*, 106953.
(37) Ramani, A.; Dahoe, A. E. On flame retardancy in polycaprolactam composites by aluminium diethylphosphinate and melamine polyphosphate in conjunction with organically modified montmorillonite nanoclay. *Polym. Degrad. Stabil.* **2014**, *105*, 1−11.
(38) Liu, J.; Dong, C. H.; Zhang, Z.; Sun, H.; Kong, D. Z.; Lu, Z. Durable flame retardant cotton fabrics modified with a novel silicon-phosphorus-nitrogen synergistic flame retardant. *Cellulose* **2020**, *27*, 9027−9043.
(39) Zhu, S. J.; Gong, W. G.; Luo, J.; Meng, X.; Xin, Z.; Wu, J.; Jiang, Z. W. Flame Retardancy and Mechanism of Novel Phosphorus-Silicon Flame Retardant Based on Polysilsesquioxane. *Polymers* **2019**, *11*, 1304.
(40) Harada, M.; Morioka, D.; Ochi, M. Thermal and mechanical properties of tetra-functional mesogenic type epoxy resin cured with aromatic amine. *J. Appl. Polym. Sci.* **2018**, *135*, 46181.
(41) Fang, L. X.; Zhou, J. F.; Wang, J. J.; Sun, J.; Fang, Q. A Bio-Based Allylphenol (Eugenol)-Functionalized Fluorinated Maleimide with Low Dielectric Constant and Low Water Uptake. *Macromol. Chem. Phys.* **2018**, *219*, 1800252.
(42) Han, C. S. Influence of the molecular structure on indentation size effect in polymers. *Mater. Sci. Eng., A* **2010**, *527*, 619−624.
(43) Hua, F. F.; Liu, D. B. On dissipative gradient effect in higher-order strain gradient plasticity: the modelling of surface passivation. *Acta Mech. Sin.* **2020**, *36*, 840−854.
(44) Fan, L.; Zhang, S. B.; Li, X.; Hu, H.; Huang, Y. W.; Ma, J. J.; Yang, J. X. Room-temperature photopatternable low-dielectric cured resins derived from siloxane-carbosilane hybridized polymers. *J. Mater. Chem. C* **2019**, *7*, 1518−1524.
(45) Weng, L.; Zhang, Y. C.; Zhang, X. R.; Liu, L. Z.; Zhang, H. X. Synthesis and properties of cyanate mixed resin systems modified by polyphenylene oxide for production of high-frequency copper clad laminates. *J. Mater. Sci. Mater. Electron.* **2018**, *29*, 2831−2840.
(46) Weng, L.; Zhang, Y. C.; Zhang, X. R.; Liu, L. Z.; Zhang, H. X. Synthesis and properties of cured epoxy mixed resin systems modified by polyphenylene oxide for production of high-frequency copper clad laminates. *Polym. Compos.* **2018**, *39*, E2334−E2345.
(47) Li, J. Y.; Zhang, Z. Y.; Zhu, T. W.; Li, Z.; Wang, J. Y. R.; Cheng, Y. Multi-benzocyclobutene functionalized siloxane monomers prepared by Piers-Rubinsztajn reaction for low-k materials. *Eur. Polym. J.* **2020**, *126*, 109562.

https://doi.org/10.1021/acsomega.2c08159
ACS Omega 2023, 8, 9464−9474